Supplementary

PbI_2 Nanocrystalline Coated on Cellulose Fiber Frame for Paper-based Flexible X-ray Detection

Hui Sun[1*], Qianfa Su[,2], Shuo Wang[3], Yizhen Liu[2], Xiuying Gao[1], Qiya Liu[1], Chuan Tang[1], Tixian Zeng[1] and Dingyu Yang[1]

1. College of Optoelectronic Engineering, Key Laboratory of Information Material and Device Application of Sichuan Province, Chengdu University of Information Technology, Chengdu, 610225, China

2. School of Materials and Energy, University of Electronic Science and Technology of China, Chengdu, 611731, China

3. College of Biophotonics, South China Normal University, Guangzhou, 510631, China

*Corresponding author: Dr. H. Sun, email: *sunhui@cuit.edu.cn*

Keywords: Flexible X-ray detector, PbI_2 nanocrystalline, Paper electronic, Direct-conversion, Photoconductor, Cellulose fiber frame

S1: Charge collection efficiency (CCE)

The μτ product can be derived from Hecht fitting with photocurrent density−voltage curves, as shown in Figure S2. The Hecht equation,

$$\frac{I}{I_0}=\frac{\mu\tau V}{L^2}(1-(\exp\left(-\frac{L^2}{\mu\tau V}\right))$$

where I_0 is the saturated photocurrent, I is the total current, V is the voltage and L is the distance between bias electrode and signal electrode.

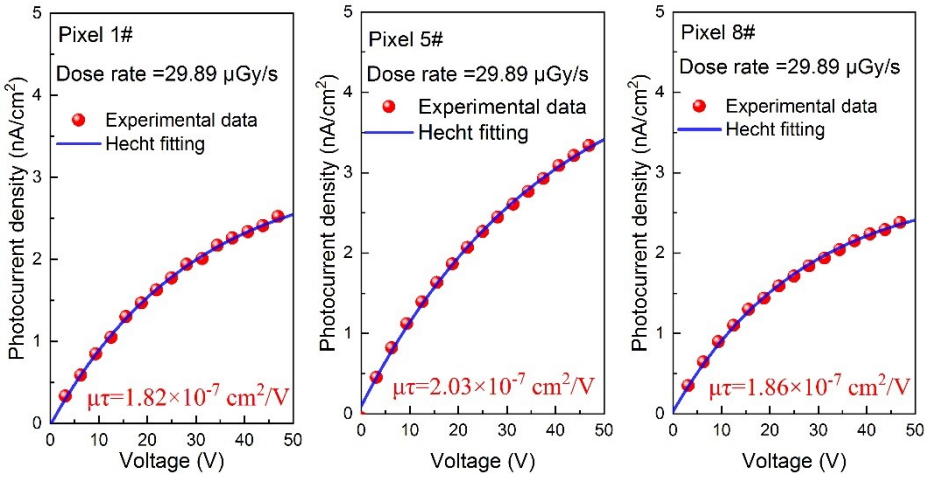

Figure S1. Hecht fitting with photocurrent density−voltage curves for Pixel 1#, 5# and 8#.

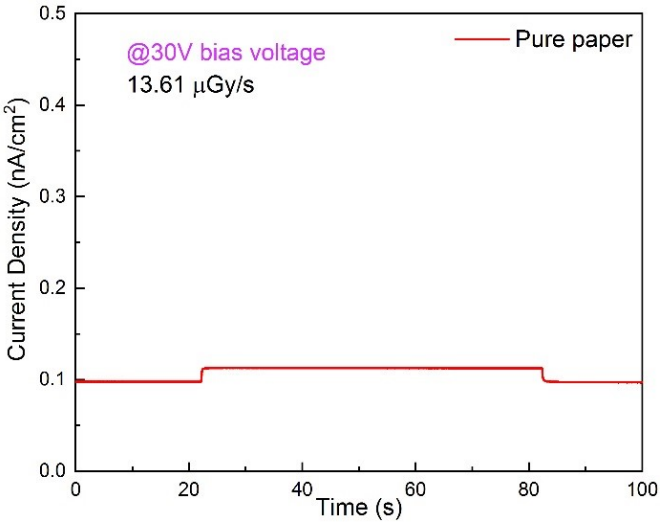

Figure S2. The response current of the pure paper without PbI_2 nanocrystalline loaded.

S2: SNR calculation process

the signal-to-noise ratio (SNR) is mainly determined by the fluctuation of the photocurrent, the calculation process shown as follows:

$$SNR = \frac{I_{signal}}{I_{noise}} \quad (1)$$

The signal current (I_{signal}) was derived by subtracting the average photocurrent ($\bar{I}_{photo}$) by the average dark current ($\bar{I}_{dark}$). The noise current ($\bar{I}_{noise}$) was obtained by calculating the standard deviation of the photocurrent.

$$I_{signal} = \bar{I}_{photo} - \bar{I}_{dark} \quad (2)$$

$$\bar{I}_{noise} = \sqrt{\frac{1}{N}\sum_{i}^{N}(I_i - \bar{I}_{photo})^2} \quad (3)$$

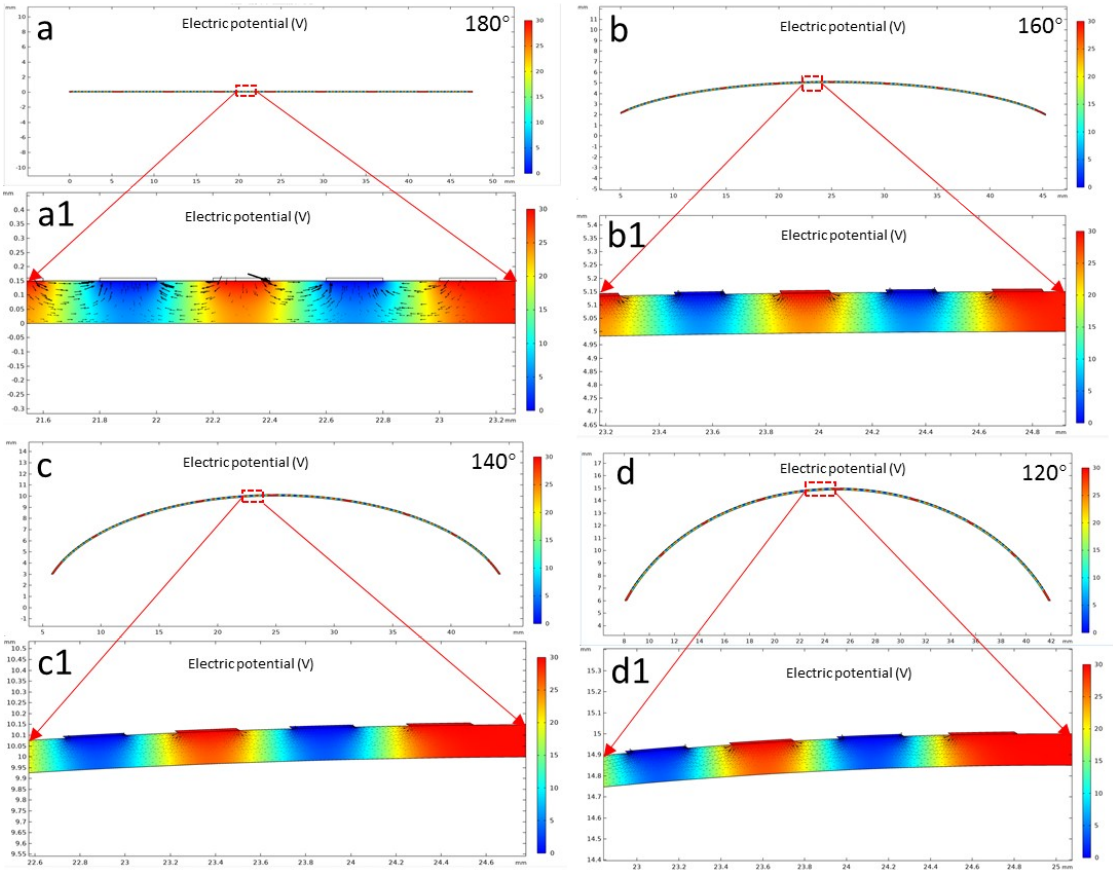

Figure S3. (a-d) Electric field distribution of different positions under different bending angles. (a1-d1) Enlarged electric field and potential distribution of Pixel 4#. Cloud maps and curves (including scissor lines) represent the potential and line distribution, respectively.

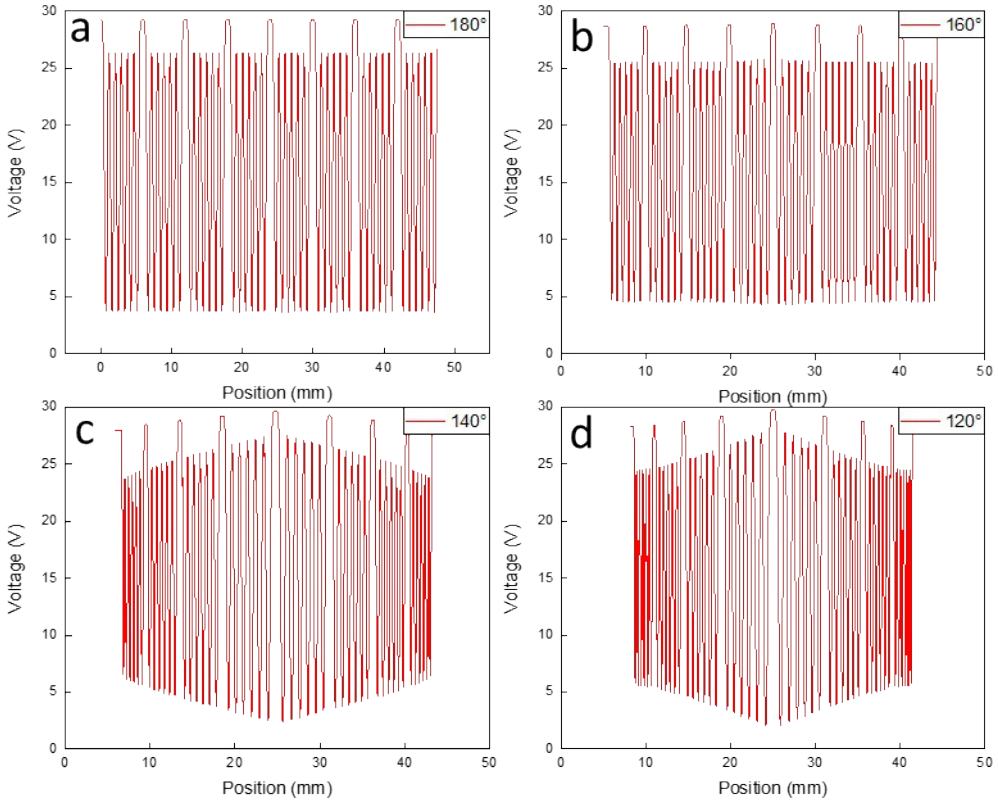

Figure S4. Detailed potential distribution of the full-size devices under different bending conditions.

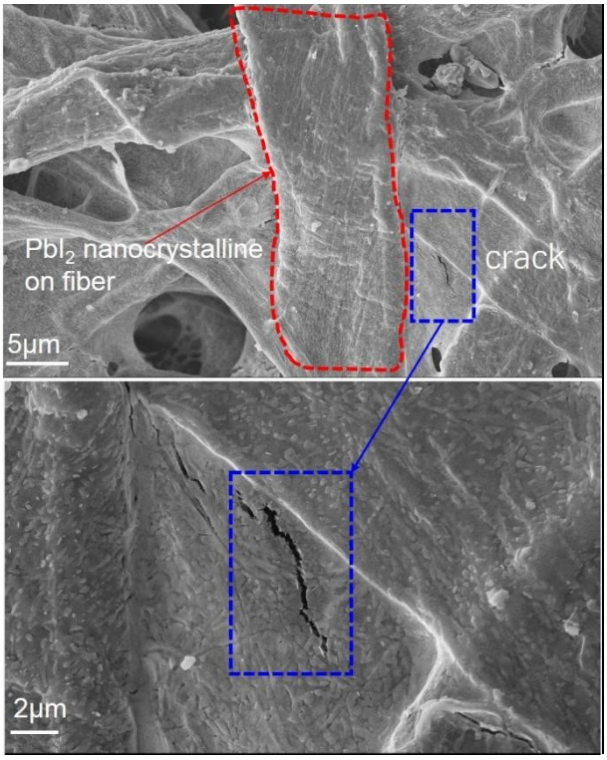

Figure S5. SEM image of the PbI_2-CFP X-ray detector after 1000 bending cycles

We built a complete linear array X-ray detector imaging system, as shown in Figure S6 and S7. This system can be considered as consisting of motion control module and data acquisition module. The motion control module is mainly composed of four parts: Weinview touch screen, Mitsubishi power line communication FX-1N (MIT PLC FX-1N), stepper motor driver and stepper motor. The data acquisition module includes an 8-pixel linear array flexible X-ray detector, an 8-channel trans-resistance operational amplifier (OPA, TLC2201), an analog-to-digital converter (ADC, ADS1256) module, a microcontroller (MCU, STM32F103C8T6) system and TFT screen. Figure S6 shows the photograph of self-built 8-channel imaging system. Figure S7 illustrates the principle of the whole system and the flow diagram of the imaging process.

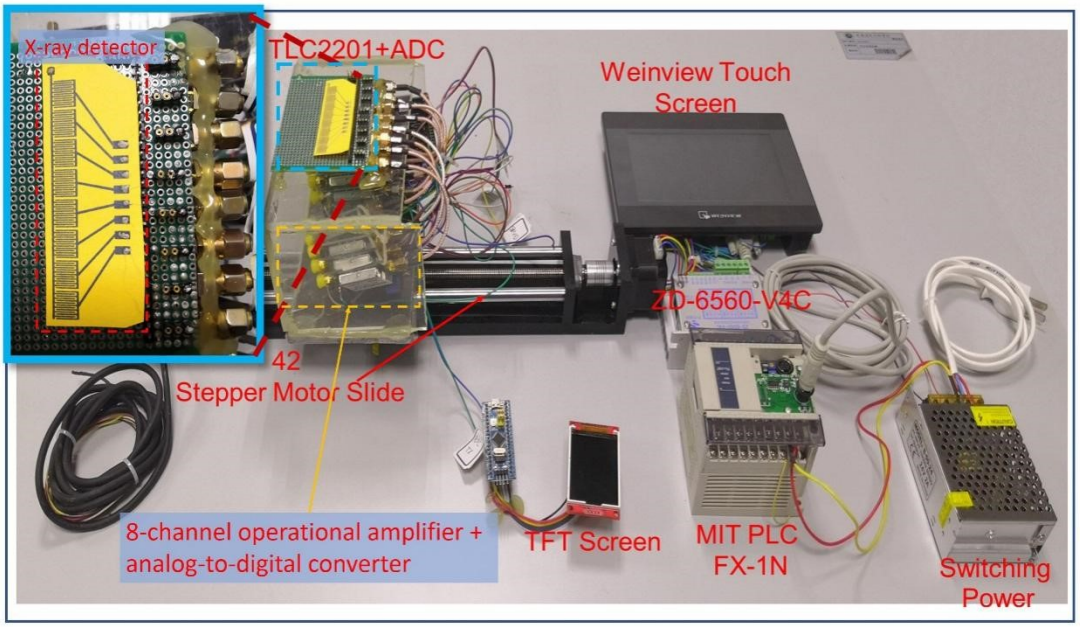

Figure S6. Photograph of self-built 8-channel imaging system

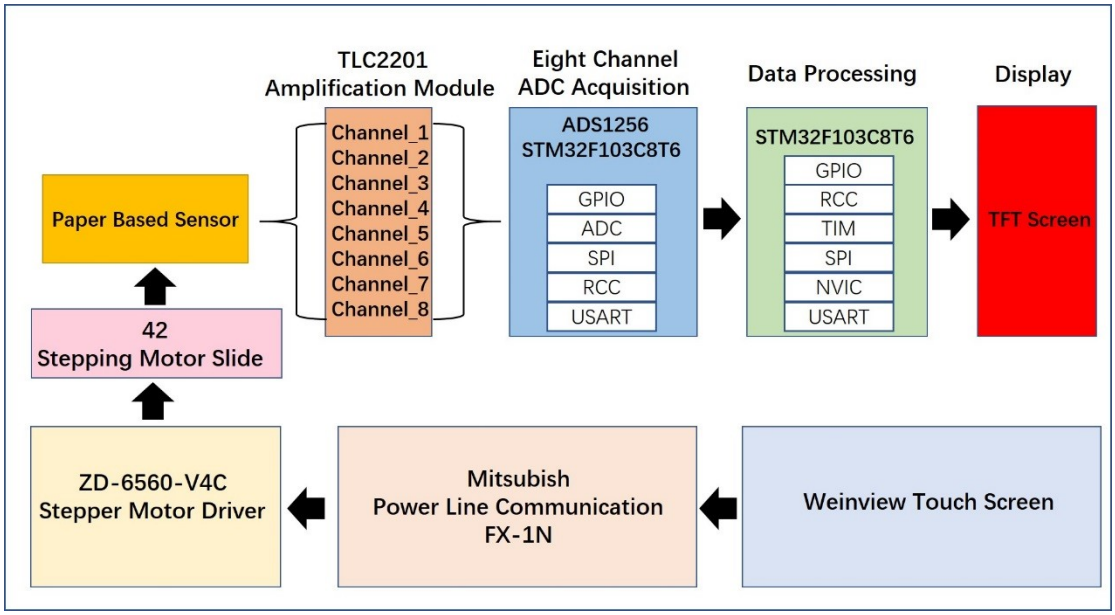

Figure S7. Flow chart based on self-built 8-channel imaging system